Journal of The Electrochemical Society, **154** (10) A910-A916 (2007)
0013-4651/2007/154(10)/A910/7/$20.00 © The Electrochemical Society

Numerical Simulation of Intercalation-Induced Stress in Li-Ion Battery Electrode Particles

Xiangchun Zhang,[a,*] Wei Shyy,[b] and Ann Marie Sastry[a,c,d,,z]**

[a]*Department of Mechanical Engineering,* [b]*Department of Aerospace Engineering,* [c]*Department of Biomedical Engineering, and* [d]*Department of Material Science and Engineering, University of Michigan, Ann Arbor, Michigan 48109-2125, USA*

Severe, particle-level strains induced during both production and cycling have been putatively linked to lifetime limiting damage in lithium-ion cells. Because of the presently unknown contributions of manufacturing and intercalation induced stresses in Li cells, this correlation is critical in determining optimal materials and manufacturing methods for these cells. Both global and localized loads must be estimated, in order to select materials able to resist fracture. Here, we select the $LiMn_2O_4$ system for study. We present results of a set of simulation techniques, ranging from one-dimensional finite difference simulations of spherical particles, to fully three-dimensional (3D) simulations of ellipsoidal particles, to systematically study the intercalation-induced stresses developed in particles of various shapes and sizes, with the latter 3D calculations performed using a commercial finite element code. Simulations of spherical particles show that larger particle sizes and larger discharge current densities give larger intercalation-induced stresses. Simulations of ellipsoidal particles show that large aspect ratios are preferred to reduce the intercalation-induced stresses. In total, these results suggest that it is desirable to synthesize electrode particles with smaller sizes and larger aspect ratios to reduce intercalation-induced stress during cycling of lithium-ion batteries.
 [DOI: 10.1149/1.2759840]

Manuscript submitted February 19, 2007; revised manuscript received May 28, 2007. Available electronically July 31, 2007.

Severe, particle-level strains induced during both production and cycling have been putatively linked to lifetime limiting damage in lithium-ion cells. Intercalation and deintercalation of Li ions into cathodic lattices, including $LiCoO_2$,[1] $LiMn_2O_4$,[2] and $LiFePO_4$,[3] have been postulated to result in fraction inside the particles, as determined by experimentation on model systems. In $LiMn_2O_4$, for example, a 6.5% percent volume change has been reported when Mn_2O_4 is lithiated into $LiMn_2O_4$;[4] simulations of $LiMn_2O_4$ suggested that intercalation-induced stress may exceed the ultimate strength of the material.[5] Also, stress generation due to cell-scale loads by compression during manufacturing has been shown to result in localized particle stresses that are much higher in the graphite anode material[6] (the ratio between local and global stresses is around 25 to 140). Indeed, stresses of these orders exceed the known strengths of these materials including the most commonly used, and most promising, cathode materials [Table I (Ref. 7, 8, 4, and 9)].

Stress generation due to Li-intercalation, and more generally in other processes, has been modeled in prior work at the particle scale. Christensen and Newman estimated stress generation in lithium insertion into the carbon anode[10] and $LiMn_2O_4$ cathode[5] particles. More broadly, stresses induced by species diffusion have been studied in other fields, including metal oxidation and semiconductor doping. Prussin[11] first treated diffusion-induced stress by analogy to thermal stress. In this study, stress generation during doping of boron and phosphorus into silicon wafer was studied. Li[12] studied diffusion-induced stress or chemical stress in elastic media of simple geometries following this method as well.[12] Yang[13] studied the evolution of chemical stress in a thin plate considering the interaction between chemical stress and diffusion following the thermal stress analogy by Prussin.[11]

Though these sets of efforts offer a means of stress estimation at the particle scale, by different physical assumptions, the implementations to date have not been applied to the problem of three-dimensional stresses. Because of the presently unknown contributions of manufacturing and intercalation-induced stresses in Li cells, this correlation is critical in determining optimal materials and manufacturing methods for these cells. Both global and localized loads must be estimated in order to select materials able to resist fracture. Further, the role of localized particle fracture in capacity fade has been implied, but not quantified, given the general lack of understanding of localized loads in batteries.

Thus, the present work is focused on determination of localized particle stresses in cathode particles. Here, we selected the $LiMn_2O_4$ system, following Ref. 14-18 on battery performance modeling, Ref. 19 and 20 on atomic scale simulations of structure, and Ref. 5 on intercalation-induced stress simulation because of the low cost and environmental safety of $LiMn_2O_4$. We have the following objectives in this study:

1. To determine diffusion-induced stresses according to an analogy to thermal stress, following Ref. 11-13 for single particles, and determine the correspondence with prior work[5] in Li cells;
2. To verify the implementation of a single-particle model numerically, using a finite difference scheme and validation of simple results; and
3. To implement this model into a full finite element scheme, and simulate stresses induced by intercalation in particles of nonspherical geometry.

Simulation

Stress-strain relations.— For intercalation processes, the lattice constants of the material may be assumed to change linearly[4] with the volume of ions inserted, which results in stresses. Therefore, one can calculate intercalation-induced stress by analogy to thermal stress. Prussin[11] previously treated concentration gradients analogously to those generated by temperature gradients in an otherwise unstressed body.

Stress-strain relations including thermal effects are written classically for an elastic body[21] as

$$\varepsilon_{xx} - \alpha T = \frac{1}{E}[\sigma_{xx} - \nu(\sigma_{yy} + \sigma_{zz})] \qquad [1a]$$

Table I. Stress and strain in cathode materials in the intercalation process.

Material	Measurement technique	Stress or strain
$LiCoO_2$ film (Ref. 7)	Laser beam deflection	~1 GPa (stress)
$LiMn_2O_4$ film (Ref. 8)	Laser beam deflection	~0.64 GPa (stress)
$LiMn_2O_4$ (Ref. 4)	Neutron-diffraction	0.027 (strain)
$LiFePO_4$ (Ref. 9)	X-ray diffraction	0.022 (strain)

* Electrochemical Society Student Member.
** Electrochemical Society Active Member.
z E-mail: amsastry@umich.edu

$$\varepsilon_{yy} - \alpha T = \frac{1}{E}[\sigma_{yy} - \nu(\sigma_{xx} + \sigma_{zz})] \quad [1b]$$

$$\varepsilon_{zz} - \alpha T = \frac{1}{E}[\sigma_{zz} - \nu(\sigma_{xx} + \sigma_{yy})] \quad [1c]$$

$$\varepsilon_{xy} = \frac{\sigma_{xy}}{2G} \quad \varepsilon_{yz} = \frac{\sigma_{yz}}{2G} \quad \varepsilon_{xz} = \frac{\sigma_{xz}}{2G} \quad [1d]$$

where ε_{ij} are strain components, σ_{ij} are stress components, E is Young's modulus, ν is Poisson's ratio, G is modulus of elasticity in shear, α is thermal expansion coefficient, and T is the temperature change from the original value. Analogously, the stress-strain relation with the existing of concentration gradients can be written as[13]

$$\varepsilon_{ij} = \frac{1}{E}[(1 + \nu)\sigma_{ij} - \nu\sigma_{kk}\delta_{ij}] + \frac{\tilde{c}\Omega}{3}\delta_{ij} \quad [2]$$

where $\tilde{c} = c - c_0$ is the concentration change of the diffusion species from the original (stress-free) value, and Ω is partial molar volume of solute. Equation 2 can be rewritten to obtain the expression for the components of stresses

$$\sigma_{ij} = 2\mu\varepsilon_{ij} + (\lambda\varepsilon_{kk} - \beta\tilde{c})\delta_{ij} \quad [3]$$

where $\mu = E/2(1 + \nu)$, $\lambda = 2\nu\mu/(1 - 2\nu)$, and $\beta = \Omega(3\lambda + 2\mu)/3$. As usual in elasticity, the strain tensor is related to displacement **u** as[21]

$$\varepsilon_{ij} = \frac{1}{2}\left(\frac{\partial u_i}{\partial x_j} + \frac{\partial u_j}{\partial x_i}\right) \quad [4]$$

and the equilibrium equation, neglecting body forces, is[21]

$$\sigma_{ij,i} = 0 \quad (j = 1,2,3) \quad [5]$$

Substitution of Eq. 3 and 4 into Eq. 5 leads to the displacement equations[22]

$$\mu\nabla^2 u_i + (\lambda + \mu)u_{k,ki} - \beta\tilde{c}_{,i} = 0 \quad (i = 1,2,3) \quad [6]$$

The boundary condition for the case of a single particle is that the particle surface is traction-free. This condition can be expressed as[22]

$$p_{nx} = \sigma_{xx}l + \sigma_{yx}m + \sigma_{zx}n = 0 \quad [7a]$$

$$p_{ny} = \sigma_{xy}l + \sigma_{yy}m + \sigma_{zy}n = 0 \quad [7b]$$

$$p_{nz} = \sigma_{xz}l + \sigma_{yz}m + \sigma_{zz}n = 0 \quad [7c]$$

where l,m,n denote the direction cosines between the external normal and each axis. Substitution of Eq. 3 and 4 into boundary conditions Eq. 7 yields

$$\mu(u_{i,j} + u_{j,i})n_j + (\lambda u_{k,k} - \beta c)n_i = 0 \quad i = 1,2,3 \quad [8]$$

where $n_1 = l$, $n_2 = m$ and $n_3 = n$. Therefore, we are left to solve Eq. 6, with the boundary condition of Eq. 8.

Diffusion equation.— As shown in Eq. 2 and 3, concentrations are needed to calculate intercalation-induced stresses. To obtain a concentration profile, the insertion and extraction of ions are modeled as a diffusion process. The effect of existing electrons in the solid on the species flux of lithium can be neglected, because electrons are much more mobile than intercalated atoms.[23] The chemical potential gradient is the driving force for the movement of lithium ions. The velocity of lithium ions can be expressed as

$$\mathbf{v} = -M\nabla\mu \quad [9]$$

where M is the mobility of lithium ions, and μ is the chemical potential. The species flux can then be written as[23]

$$\mathbf{J} = c\mathbf{v} = -Mc\nabla\mu \quad [10]$$

where c is the concentration of the diffusion component (lithium ions).

The electrochemical potential in an ideal solid solution can be expressed as[13,24]

$$\mu = \mu_0 + RT\ln X - \Omega\sigma_h \quad [11]$$

where μ_0 is a constant, R is gas constant, T is absolute temperature, X is the molar fraction of lithium ion, Ω is partial molar volume of lithium ion, and σ_h is the hydrostatic stress, which is defined as $\sigma_h = (\sigma_{11} + \sigma_{22} + \sigma_{33})/3$ (where σ_{ij} are the elements in stress tensor). Equations 10 and 11 show that the diffusion flux depends on concentration, temperature, and stress field. Substitution of Eq. 11 into Eq. 10, assuming temperature is uniform, and noting that

$$\nabla(RT\ln X) = RT\frac{1}{X}\nabla X = RT\frac{1}{c}\nabla c \quad [12]$$

an expression of species flux (when there is no temperature gradient inside the particle) can be obtained as

$$\mathbf{J} = -D\left(\nabla c - \frac{\Omega c}{RT}\nabla\sigma_h\right) \quad [13]$$

where $D = MRT$ is diffusion coefficient. Conservation of species gives

$$\frac{\partial c}{\partial t} + \nabla\cdot\mathbf{J} = 0 \quad [14]$$

Then, substituting Eq. 13 into Eq. 14 gives finally

$$\frac{\partial c}{\partial t} = D\left(\nabla^2 c - \frac{\Omega}{RT}\nabla c\cdot\nabla\sigma_h - \frac{\Omega c}{RT}\nabla^2\sigma_h\right) \quad [15]$$

as the governing equation for the diffusion process. The initial condition is $c = c_0$, with the boundary condition

$$\mathbf{J} = -D\left(\nabla c - \frac{\Omega c}{RT}\nabla\sigma_h\right) = \frac{i_n}{F} \quad [16]$$

where i_n is the current density on the particle surface (which is assumed to be a constant, known value in this study), and F is Faraday's constant.

Numerical methods.— Finite difference method for 1D problem.— For the case of a spherical particle, the above equations become one-dimensional. The stress tensor contains two independent components, radial stress σ_r and tangential stress σ_t. The equilibrium equation (refer to Eq. 5) for this case is simply

$$\frac{d\sigma_r}{dr} + \frac{2}{r}(\sigma_r - \sigma_t) = 0 \quad [17]$$

and the stress-strain relations (referring to Eq. 2) are

$$\varepsilon_r = \frac{1}{E}(\sigma_r - 2\nu\sigma_t) + \frac{\Omega}{3}\tilde{c} \quad [18]$$

$$\varepsilon_t = \frac{1}{E}[\sigma_t - \nu(\sigma_r + \sigma_t)] + \frac{\Omega}{3}\tilde{c} \quad [19]$$

The strain-displacement relations (referring to Eq. 4) are

$$\varepsilon_r = \frac{du}{dr} \quad \varepsilon_t = \frac{u}{r} \quad [20]$$

and the displacement equation (refer to Eq. 6) is

$$\frac{d^2u}{dr^2} + \frac{2}{r}\frac{du}{dr} - \frac{2u}{r^2} = \frac{1 + \nu}{1 - \nu}\frac{\Omega}{3}\frac{d\tilde{c}}{dr} \quad [21]$$

Integration of this equation yields a solution for u, from which stresses may be obtained. Noting that stresses are finite at the center of the sphere ($r = 0$), and that radial stresses are zero, $\sigma_r = 0$, at the particle surface ($r = r_0$), the two constants in the solution can be determined as

$$\sigma_r = \frac{2\Omega E}{3(1-\nu)}\left(\frac{1}{r_0^3}\int_0^{r_0}\tilde{c}r^2\mathrm{d}r - \frac{1}{r^3}\int_0^{r}\tilde{c}r^2\mathrm{d}r\right) \quad [22]$$

and

$$\sigma_t = \frac{\Omega E}{3(1-\nu)}\left(\frac{2}{r_0^3}\int_0^{r_0}\tilde{c}r^2\mathrm{d}r + \frac{1}{r^3}\int_0^{r}\tilde{c}r^2\mathrm{d}r - \tilde{c}\right) \quad [23]$$

Equation 22 shows that radial stress actually depends upon the difference between the global and local averages of concentration.

The diffusion equation is (referring to Eq. 15)

$$\frac{\partial c}{\partial t} = D\left[\frac{\partial^2 c}{\partial r^2} + \frac{2}{r}\frac{\partial c}{\partial r} - \frac{\Omega}{RT}\frac{\partial c}{\partial r}\frac{\partial \sigma_h}{\partial r} - \frac{\Omega c}{RT}\left(\frac{\partial^2 \sigma_h}{\partial r^2} + \frac{2}{r}\frac{\partial \sigma_h}{\partial r}\right)\right] \quad [24]$$

Equations 22 and 23 allow calculation of hydrostatic stress as

$$\sigma_h = (\sigma_r + 2\sigma_t)/3 = \frac{2\Omega E}{9(1-\nu)}\left(\frac{3}{r_0^3}\int_0^{r_0}\tilde{c}r^2\mathrm{d}r - \tilde{c}\right) \quad [25]$$

By assuming that the characteristic time for elastic deformation of solids is much smaller than that for atomic diffusion, the elastic deformation can be treated as quasistatic.[13] Therefore, Eq. 25 can be substituted into Eq. 24 to obtain

$$\frac{\partial c}{\partial t} = D\left[\frac{\partial^2 c}{\partial r^2} + \frac{2}{r}\frac{\partial c}{\partial r} + \theta\left(\frac{\partial c}{\partial r}\right)^2 + \theta c\left(\frac{\partial^2 c}{\partial r^2} + \frac{2}{r}\frac{\partial c}{\partial r}\right)\right] \quad [26]$$

where $\theta = (\Omega/RT)[(2\Omega E)/9(1-\nu)]$.

Substituting Eq. 25 into boundary conditions Eq. 16, one has

$$\mathbf{J} = -D(1+\theta c)\frac{\partial c}{\partial r} = \frac{i_n}{F} \quad \text{at } r = r_0 \quad [27]$$

In this way, the two variables, concentration and stress, are decoupled.

To solve the above equation numerically, it is, along with boundary and initial condition, transformed into dimensionless form first as

$$\frac{\partial \hat{c}}{\partial \hat{t}} = \frac{\partial^2 \hat{c}}{\partial \hat{r}^2} + \frac{2}{r}\frac{\partial \hat{c}}{\partial \hat{r}} + \hat{\theta}\left(\frac{\partial \hat{c}}{\partial \hat{r}}\right)^2 + \hat{\theta}\hat{c}\left(\frac{\partial^2 \hat{c}}{\partial \hat{r}^2} + \frac{2}{\hat{r}}\frac{\partial \hat{c}}{\partial \hat{r}}\right) \quad [28]$$

$$0 \le \hat{r} \le 1 \quad 0 \le \hat{t} \le \hat{T} \quad [\text{where } \hat{T} \text{ satisfies } \hat{c}(\hat{r}=1,\hat{t}=\hat{T}) = 1]$$

$$\hat{r} = 1 - (1+\hat{\theta}\hat{c})\frac{\partial \hat{c}}{\partial \hat{r}} = I \quad \hat{r} = 0 \quad \frac{\partial \hat{c}}{\partial \hat{r}} = 0$$

$$\hat{t} = 0 \quad \hat{c} = c_0/c_{\max}$$

where dimensionless variables are defined as

$$\hat{r} = \frac{r}{r_0} \quad \hat{t} = \frac{tD}{r_0^2} \quad \hat{c} = \frac{c}{c_{\max}} \quad \hat{\theta} = \theta c_{\max} \quad I = \frac{i_n r_0}{D c_{\max} F}$$

In the above equations, $c_{\max}$ is the stoichiometric maximum concentration and c_0 is the initial concentration. It may be seen that the effect of discharge current density, particle radius, and diffusion coefficient are all combined into the dimensionless current density I.

The numerical procedure is as follows. For each time step, concentration distribution is solved first by Eq. 28. Then, the concentration is substituted into Eq. 22 and 23 to calculate stresses. Equation 28 is a nonlinear, parabolic partial differential equation. The finite difference method is used here to solve the equation.

First, Eq. 28 is rewritten as

$$\frac{\partial \hat{c}}{\partial \hat{t}} = (1+\theta\hat{c})\frac{\partial^2 \hat{c}}{\partial \hat{r}^2} + \left(\frac{2}{\hat{r}} + \hat{\theta}\frac{\partial \hat{c}}{\partial \hat{r}} + \frac{2\hat{\theta}\hat{c}}{\hat{r}}\right)\frac{\partial \hat{c}}{\partial \hat{r}} \quad [29]$$

To discretize the differential equation into difference equations, the problem is linearized by taking the value from the previous time step for the terms in the two parentheses on the right side. The Crank-Nicolson method is used for other terms. The difference equation obtained is

$$\frac{\hat{c}_i^{n+1} - \hat{c}_i^n}{\Delta\hat{t}} = (1+\hat{\theta}\hat{c}_i^n)\frac{(\hat{c}_{i+1}^{n+1} + \hat{c}_{i-1}^{n+1} - 2\hat{c}_i^{n+1}) + (\hat{c}_{i+1}^{n} + \hat{c}_{i-1}^{n} - 2\hat{c}_i^{n})}{2(\Delta\hat{r})^2} + \left(\frac{2}{\hat{r}_i} + \hat{\theta}\frac{\hat{c}_{i+1}^n - \hat{c}_{i-1}^n}{2\Delta\hat{r}} + \frac{2}{\hat{r}_i}\hat{\theta}\hat{c}_i^n\right)\frac{(\hat{c}_{i+1}^{n+1} - \hat{c}_{i-1}^{n+1}) + (\hat{c}_{i+1}^{n} - \hat{c}_{i-1}^{n})}{2(2\Delta\hat{r})} \quad [30]$$

Terms including $1/\hat{r}$ will be singular at the particle center $\hat{r} = 0$. To solve this difficulty, noting that

$$\frac{\partial \hat{c}}{\partial \hat{r}} = 0 \quad \text{when } \hat{r} = 0 \quad [31]$$

L'Hopital's rule

$$\lim_{\hat{r}\to 0}\frac{1}{\hat{r}}\frac{\partial \hat{c}}{\partial \hat{r}} = \frac{\partial^2 \hat{c}}{\partial \hat{r}^2} \quad [32]$$

can be used to eliminate the $1/\hat{r}$ factor. Thus, Eq. 28 becomes

$$\frac{\partial \hat{c}}{\partial \hat{t}} = (3+3\hat{\theta}\hat{c})\frac{\partial^2 \hat{c}}{\partial \hat{r}^2} + \left(\hat{\theta}\frac{\partial \hat{c}}{\partial \hat{r}}\right)\frac{\partial \hat{c}}{\partial \hat{r}} \quad [33]$$

which has no singularity at $\hat{r} = 0$. Therefore, Eq. 33 will be solved at $\hat{r} = 0$ while Eq. 29 is solved elsewhere.

At two boundary points, imaginary points (out of the boundary) are used to discretize the governing equation; the concentration values of these imaginary points are obtained by central differencing of the flux boundary condition at the boundary points.

The Thomas algorithm is used to solve the tridiagonal system of the difference equations. The simulation is halted when the concentration on the particle surface $\hat{r} = 1$ reaches the stoichiometric maximum.

Finite element method for 3D problem.— The 3D problem was simulated using FEMLAB (COMSOL Multiphysics). Two models are included in the multiphysics simulation, PDE (partial differential equation) model (general form) and solid stress-strain model. In PDE model, the diffusion process is described by the generalized form

$$\frac{\partial c}{\partial t} + \nabla \cdot \Gamma = 0 \quad [34]$$

where

$$\Gamma = -D\left(\nabla c - \frac{\Omega c}{RT}\nabla \sigma_h\right) \quad [35]$$

In the solid stress-strain model, "thermal expansion" is included as a load based on the variable of concentration c instead of temperature in thermal stress calculation.

Table II. Material properties of Mn_2O_4.

Parameter	Symbol and dimensions	Value
Young's modulus	E (GPa)	10 (Ref. 25)
Poisson's ratio	ν	0.3 (Ref. 25)
Diffusion coefficient	D (m^2/s)	7.08×10^{-15} (Ref. 5)
Partial molar volume	Ω (m^3/mol)	3.497×10^{-6}
Stoichiometric maximum concentration	$c_{\max}$ (mol/m^3)	2.29×10^4

Material properties.— All the material properties used in the simulation for Mn_2O_4 are listed in Table II.[5,25] From Eq. 2, we see that that partial molar volume plays a role analogous to a thermal

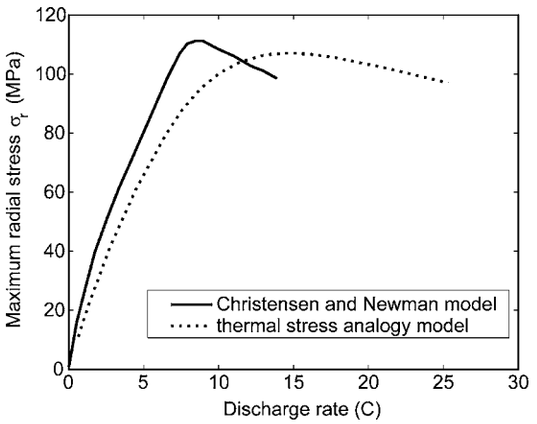

Figure 1. Comparison of simulation results of two models.

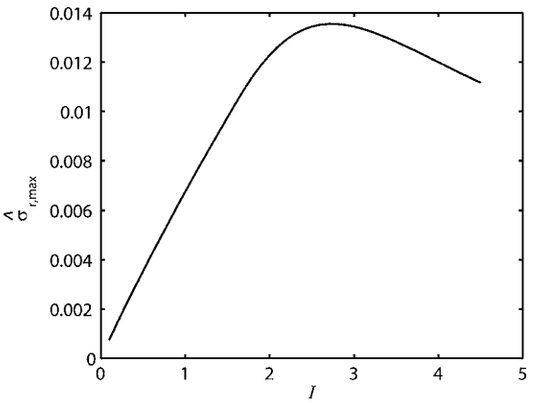

Figure 2. Maximum dimensionless radial stress vs dimensionless current density.

expansion coefficient, in calculating intercalation-induced stress. To obtain the value for this property, the volume change of 6.5% for $y = 0.2$ to $y = 0.995$ of $Li_yMn_2O_4$ is used.[5] The volume change of 6.5% gives a strain of 0.0212, which corresponds to the concentration change as $y = 0.2$ to $y = 0.995$. Therefore, partial molar volume is, by noting the analogy between thermal expansion coefficient and $\Omega/3$

$$\Omega = \frac{0.0212 \times 3}{(0.995 - 0.2)c_{\max}} = 3.497 \times 10^{-6}\ \mathrm{m^3/mol}$$

Results and Discussion

1D finite difference simulations.— Christensen and Newman[5] modeled the stress generated in $Li_yMn_2O_4$ during lithium intercalation on the 4 V plateau ($0.2 < y < 1$). The same parameters and properties are used here, except for the diffusion coefficient. In their simulation, they used a state of charge-dependent diffusion coefficient, which includes a binary interaction parameter and a thermodynamic factor. Here, a constant diffusion coefficient, taking the value of the reference binary interaction parameter in their paper, is used. The simulation results from the thermal stress analogy model and the Christensen and Newman model are shown in Fig. 1. Although different approaches are applied to calculate the intercalation-induced stress, the results qualitatively show the same trend.

We used the 1D model to simulate cycling of the active material between $y = 0$ and $y = 1$, giving an initial condition for Eq. 26 of $c_0 = 0$. Results show that that maximum radial stress is located at the center of the particle. The magnitude of the spatial maximum dimensionless radial stress is given by

$$\hat{\sigma}_{r,\max} = \frac{\sigma_{r,\max}}{E} = \frac{2\Omega c_{\max}}{3(1-\nu)}\left(\int_0^1 \hat{c}\hat{r}^2 \mathrm{d}\hat{r} - \left.\frac{1}{3}\hat{c}\right|_{\hat{r}=0}\right) \qquad [36]$$

Figure 2 shows how dimensionless maximum radial stress $\hat{\sigma}_{r,\max}$ (both temporally and spatially during the discharge process) varies with dimensionless current density (or dimensionless boundary flux) I.

As shown in Fig. 2, maximum radial stress (spatially and temporally) inside an electrode particle during the discharge process increases with increasing dimensionless current density when $0 < I < 2.7$. However, maximum radial stress decreases with increasing dimensionless current density when it is larger than 2.7. The decrease in stress is attributable to the fact that the concentration profile is not fully developed, so that the global average term (first term in the parentheses) in Eq. 36 decreases with dimensionless current density, while the local average (second term in the parenthesis) remains constant. This is not desirable in the cycling of batteries, because it reduces the utilization of the material. Therefore, only the increasing branch of the curve is actually feasible. The increasing branch shows that increase of discharge current density and particle radius will increase the intercalation-induced stress. In other words, smaller particles should be used to reduce intercalation-induced stresses.

As mentioned earlier, the model used here to simulate the intercalation-induced stress is a diffusion-stress coupling model. The effect of stress on diffusion will be discussed briefly using the 1D equations for a spherical particle. Substituting Eq. 25 into Eq. 13, we obtain

$$\mathbf{J} = -D(1 + \theta c)\frac{\partial c}{\partial r} \qquad [37]$$

In Eq. 37, θc is always a positive number, and the effective diffusion coefficient is essentially $D(1 + \theta c) > D$. Therefore, the diffusion is enhanced due to the extra term θc, which basically comes from the hydrostatic stress gradient term in Eq. 13. In other words, stress enhances the diffusion. This stress enhancement effect is also demonstrated numerically, as shown in Fig. 3. It shows the concentration profile at $t = 1000$ s with discharge current density $i = 2\ \mathrm{A/m^2}$ on the surface. The profile including the effect of stress has a smaller gradient than that excluding the stress effect, confirming that stress enhances diffusion.

Substituting the material properties into the expression of $\theta = 2\Omega^2 E/[9(1-\nu)RT]$, we obtain $\theta = 1.557 \times 10^{-5}\ \mathrm{m^3/mol}$. If the maximum concentration is used, $\theta c_{\max} = 0.356$, which is not negli-

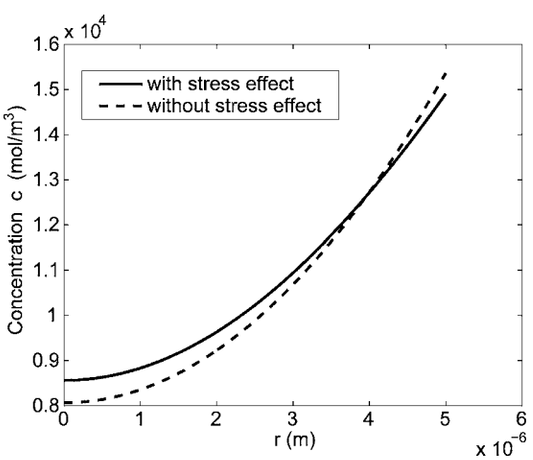

Figure 3. Numerical results for the effects of stress.

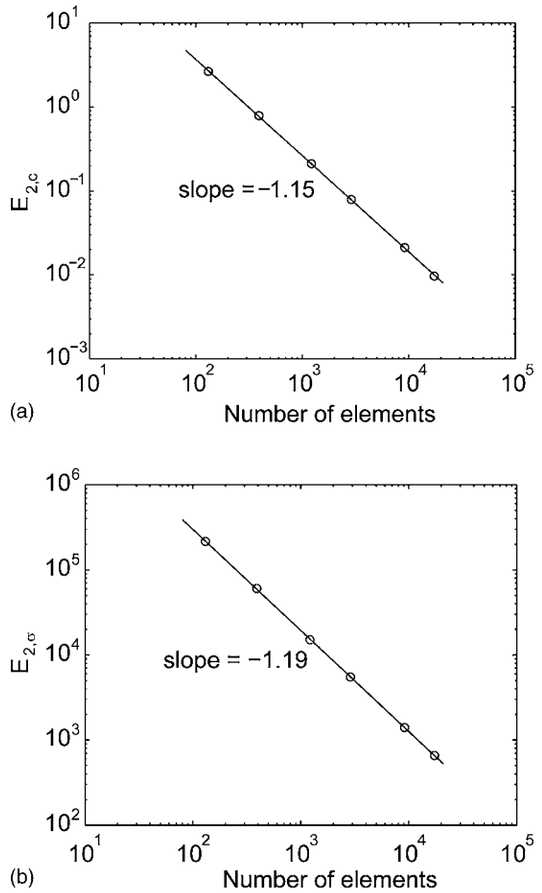

Figure 4. Convergence plot of finite element solutions for (a) hydrostatic stress and (b) concentration.

gible compared to unity. Therefore, stress effect cannot be neglected here for the case of $LiMn_2O_4$. From the expression for θ, it can be observed that θ has smaller magnitude when the material has smaller modulus E and smaller partial molar volume Ω. Thus, the stress effect on diffusion may be negligible when the material is soft (i.e., having a low modulus).

3D finite element simulation results.— The 1D finite difference simulation, with 4001 grid points and a time step of 0.001 s, was used as the reference solution to study the convergence of the finite element method. Figure 4 shows the 2-norm errors (differences) between the finite element solutions and finite difference reference solutions at $t = 1000$ s. The parameters used in the simulations are current density $i = 2$ A/m^2, and particle radius $r_0 = 5$ μm. The finite element solutions converged to the reference solution as the number of elements used increased. At the same time, Fig. 4 also shows that solutions from 1D finite difference method and 3D finite element method were consistent, because the nondimensionalized errors of concentration and stress from 17,359 elements simulation were 6.5×10^{-7} and 1.5×10^{-5}, respectively (if nondimensionalized by the maximum values at $t = 1000$ s inside the particle).

To study the effect of aspect ratios on the intercalation-induced stress, ellipsoids with different aspect ratios were studied. The current density on the surface is fixed at $i = 2$ A/m^2. For the ellipsoid, the lengths of three semiaxes a, b, and c satisfy $a = b$, and the aspect ratio is defined as $\alpha = c/a$, as sketched in Fig. 5. The volumes of the ellipsoids were fixed at $V = 4\pi \times 5^3/3$ μm^3. A set of simulations, with different aspect ratios, was run by FEMLAB.

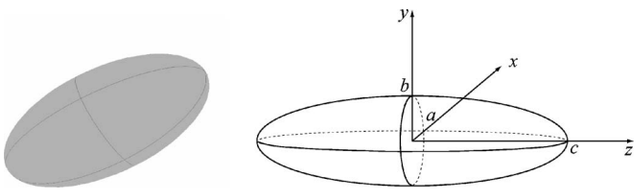

Figure 5. Schematic of an ellipsoidal particle, with coordinate system.

Characteristic solution profiles of concentration, von Mises stress and shear stress σ_{yz}, are shown in Fig. 6 at the end of the discharge process (when the surface concentration reaches the stoichiometric maximum) for an ellipsoid with aspect ratio 1.953. Figure 6 shows that (*i*) the concentration is higher around the poles, (*ii*) the von Mises stress is larger around the equator, and (*iii*) shear stress has its maximum on the surface. The solution profiles have the same patterns for other ellipsoids with different aspect ratios.

Figure 7 shows how the maximum von Mises stress inside the particle varies during the discharge process, for particles with different aspect ratios. It takes less time for particles with larger aspect ratios to completely discharge. Also, during discharge, von Mises stress increases first, and then drops. In Fig. 7, it can be observed that when aspect ratio increases, the stress increases first (for aspect ratios from 1.0 to 1.37) and then decreases (for aspect ratios from 1.37 to 3.81). For ellipsoids with aspect ratio 2.92 and 3.81, the intercalation-induced stress is smaller than that inside a sphere (aspect ratio 1.0).

Figure 8 shows how aspect ratio affects (a) peak value of maximum von Mises stress, and (b) peak value of maximum shear when the volumes of particles are fixed. Figure 8a shows that peak value of maximum von Mises stress inside the particle increases first and then decreases, as aspect ratio increases. For aspect ratios larger than 2.2, maximum von Mises stress decreases to less than that inside spherical particles (aspect ratio 1). Figure 8b shows that peak value of maximum shear stress decreases as aspect ratio increases. The results of Fig. 8 show that larger aspect ratios reduce the intercalation-induced stresses, over particles of lower aspect ratio when volume is preserved.

The peak values of maximum von Mises stresses are shown in Fig. 8a. Maximum stress first increases, then decreases with aspect ratio. This is due to two competing effects. When particle volume is preserved, increased aspect ratios result in increase of the longer semiaxis c, and reduction of shorter semiaxes a and b. Elongation of the longer semiaxis tends to increase maximum stress, while reduction of the shorter semiaxes tends to decrease the maximum stress. This competition results in a global maximum of stress at an aspect ratio of ~ 1.37.

To further illustrate the effect of semiaxes on maximum stress, an additional set of simulations was performed in which the shorter semiaxes a and b were fixed, and aspect ratio α was increased by elongation of the longer semiaxis, c. Results obtained with a discharge current density $i = 2$ A/m^2 are shown in Fig. 9. Stress first increases with aspect ratio because of the increase of the longer semiaxis, and then decreases slightly until asymptotically approaching the cylinder-fiber limit, i.e., $\alpha \to \infty$. As represented by the dashed line in Fig. 9, no physically relevant solutions are obtained for $\alpha > 7.9$, because the discharge process stops when the concentration on the particle surface reaches stoichiometric maximum, before the maximum stress actually reaches the peak value. To quantitatively illustrate this point, for an ellipsoid with aspect ratio 10, the stress reaches its peak value at $t = 721$ s. However, the simulation should terminate at $t = 617.5$ s, when the surface concentration already reaches stoichiometric maximum. The maximum stress at $t = 721$ s is 52.47 MPa, and the stress at $t = 617.5$ s is 52.26 MPa. Therefore, the stress when the process is terminated is only slightly smaller than the peak value.

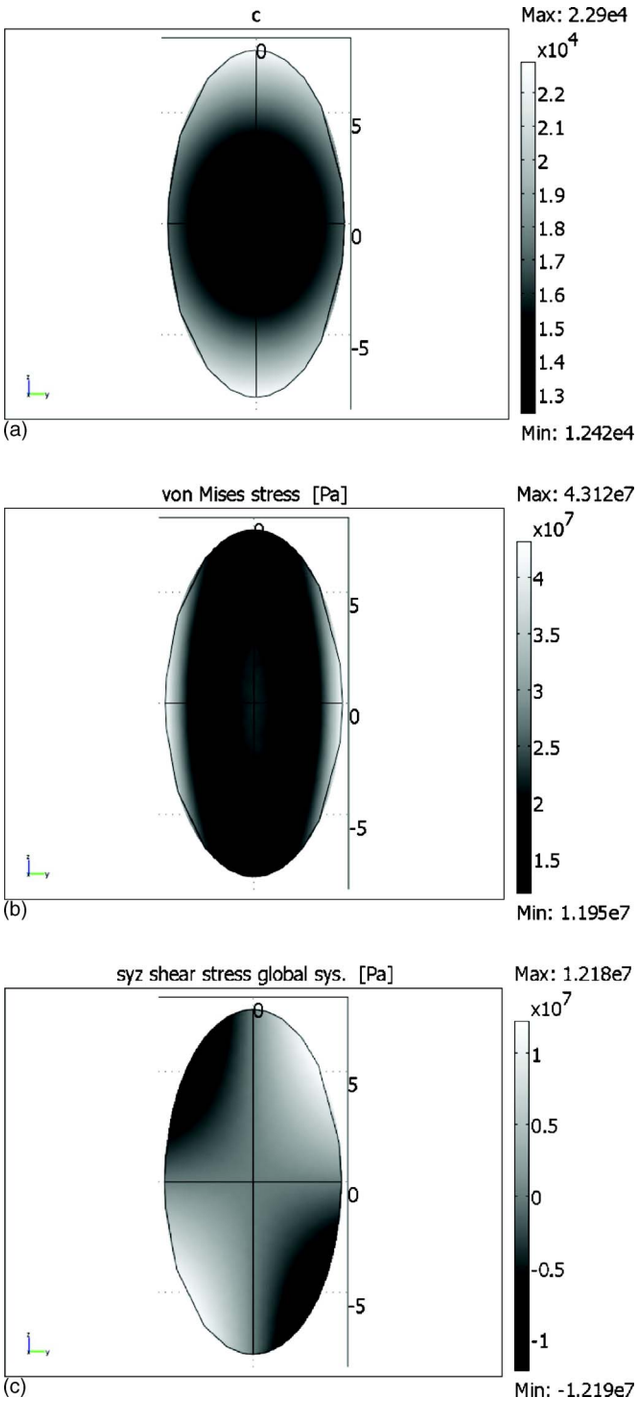

Figure 6. Solutions at the end of discharge for an ellipsoid of aspect ratio 1.953. (a) Concentration, (b) von Mises stress, and (c) shear stress σ_{yz}. (Dimensions in μm.)

Conclusion

Intercalation-induced stresses during the discharge process were simulated in this study using a stress-diffusion coupling model. Intercalation-induced stresses were simulated by analogy to thermal stress. Simulations of spherical particles show that larger particle sizes and larger discharge current densities give larger intercalation-induced stresses. Furthermore, internal stress gradients significantly enhance diffusion. Simulation results for ellipsoidal particles show that large aspect ratios are preferred to reduce the intercalation-induced stresses. In total, these results suggest that it is desirable to synthesize electrode particles with smaller sizes and larger aspect ratios to reduce intercalation-induced stress during cycling of lithium-ion batteries.

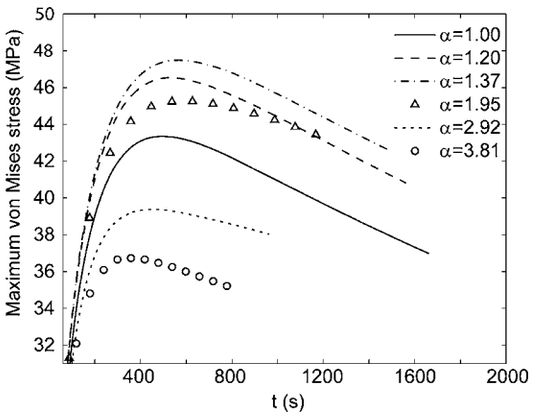

Figure 7. Maximum von Mises stress during discharge, for various ellipsoids.

Acknowledgments

The authors gratefully acknowledge the support of our sponsors, including the U.S. Department of Energy through the BATT program (Dr. Tien Duong, Program Manager), the Army Research Of-

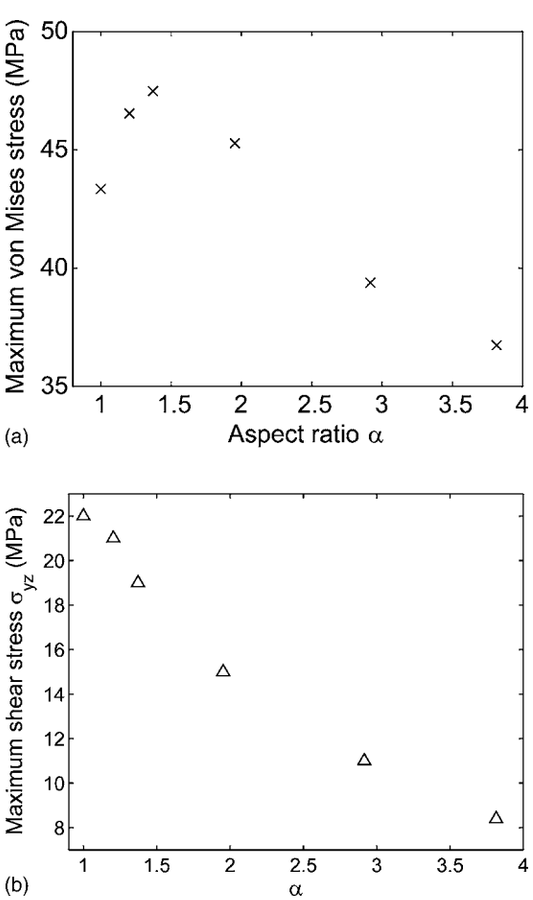

Figure 8. The effect of aspect ratio, for fixed particle volume.

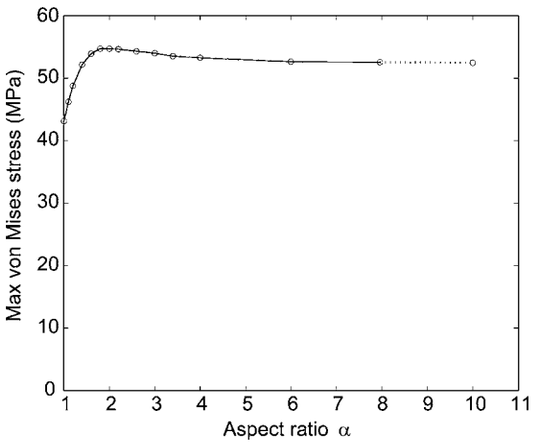

Figure 9. The effect of aspect ratio, for fixed shorter semiaxes.

fice (Dr. Bruce LaMattina, Program Manager), and the Ford Motor Company (Ted Miller and Kent Snyder, Program Managers). The authors also thank Professor James R. Barber and Dr. Chia-Wei Wang, both of the Department of Mechanical Engineering, University of Michigan, Ann Arbor, for helpful discussion and remarks.

University of Michigan assisted in meeting the publication costs of this article.

List of Symbols

a,b,c	lengths of the three semi-axes of ellipsoid, m
c	concentration of lithium ions, mol/m^3
$\tilde{c}$	concentration change from initial value, mol/m^3
D	lithium diffusion coefficient, m^2/s
E	Young's modulus, GPa
F	Faraday's constant, 96,487 C/mol
I	dimensionless current density
i_n	current density, A/m^2
$\mathbf{J}$	species flux, mol/(m^2 s)
M	mobility, m^2 mol/(J s)
R	gas constant, 8.314 J(mol K)
r_0	particle radius, μm
T	temperature, K
u	displacement, m
$\mathbf{v}$	ion movement velocity inside solid particles, m/s
X	molar fraction of lithium in the electrode

Greek

α	aspect ratio
ε_{ij}	strain
μ	chemical potential, J/mol
ν	Poisson's ratio
σ_{ij}	stress, Pa
Ω	partial molar volume, m^3/mol

Subscript

h	hydrostatic (stress)
max	maximum
r	radial direction
t	tangential direction

Others

$\wedge$	dimensionless variables

References

1. H. Wang, Y.-I. Jang, B. Huang, D. R. Sadoway, and Y.-M. Chiang, *J. Electrochem. Soc.*, **146**, 473 (1999).
2. M.-R. Lim, W.-I. Cho, and K.-B. Kim, *J. Power Sources*, **144**, 3496 (1997).
3. D. Wang, X. Wu, Z. Wang, and L. Chen, *J. Power Sources*, **140**, 125 (2005).
4. W. I. F. David, M. M. Thackeray, L. A. de Picciotto, and J. B. Goodenough, *J. Solid State Chem.*, **67**, 316 (1987).
5. J. Christensen and J. Newman, *J. Electrochem. Soc.*, **153**, A1019 (2006).
6. Y.-B. Yi, C.-W. Wang, and A. M. Sastry, *J. Eng. Mater. Technol.*, **128**, 73 (2006).
7. S.-I. Pyun, J.-Y. Go, and T.-S. Jang, *Electrochim. Acta*, **49**, 4477 (2004).
8. Y.-H. Kim, S.-I. Pyun, and J.-Y. Go, *Electrochim. Acta*, **51**, 441 (2005).
9. A. K. Padhi, K. S. Nanjundaswamy, and J. B. Goodenough, *J. Electrochem. Soc.*, **144**, 1188 (1997).
10. J. Christensen and J. Newman, *J. Solid State Electrochem.*, **10**, 293 (2006).
11. S. Prussin, *J. Appl. Phys.*, **32**, 1876 (1961).
12. J. C. M. Li, *Metall. Trans. A*, **9A**, 1353 (1978).
13. F. Yang, *Mater. Sci. Eng., A*, **409**, 153 (2005).
14. M. Doyle, J. Newman, A. S. Gozdz, C. N. Schmutz, and C. M. Tarascon, *J. Electrochem. Soc.*, **143**, 1890 (1996).
15. R. Darling and J. Newman, *J. Electrochem. Soc.*, **144**, 4201 (1997).
16. P. Arora, M. Doyle, A. S. Gozdz, R. E. White, and J. Newman, *J. Power Sources*, **88**, 219 (2000).
17. E. Deiss, D. Haringer, P. Novak, and O. Haas, *Electrochim. Acta*, **46**, 4185 (2001).
18. R. Darling and J. Newman, *J. Electrochem. Soc.*, **145**, 990 (1998).
19. C. Y. Ouyang, S. Q. Shi, Z. X. Wang, H. Li, X. J. Huang, and L. Q. Chen, *Europhys. Lett.*, **67**, 28 (2004).
20. B. Ammundsen, J Roziere, and M. S. Islam, *J. Phys. Chem. B*, **101**, 8156 (1997).
21. S. P. Timoshenko and J. N. Goodier, *Theory of Elasticity*, McGraw-Hill, New York (1970).
22. N. Noda, R. B. Hetnarski, and Y. Tanigawa, *Thermal Stresses*, 2nd ed., Taylor & Francis, New York (2003).
23. W. R. McKinnon and R. R. Haering, in *Modern Aspects of Electrochemistry*, No. 15, R. E. White, J. O'M. Bockris, and B. E. Conway, Editors, Plenum Press, New York (1983).
24. W. L. Wang, S. Lee, and J. R. Chen, *J. Appl. Phys.*, **91**, 9584 (2002).
25. A. Paolone, R. Cantelli, G. Rousse, and C. Masquelier, *J. Phys.: Condens. Matter*, **15**, 457 (2003).